Quantum Coherence and Disorder-Specific Effects in Simulations of 2D Optical Spectra of One-Dimensional J-aggregates

ARTICLE *in* THE JOURNAL OF PHYSICAL CHEMISTRY A · MARCH 2011

Impact Factor: 2.69 · DOI: 10.1021/jp108291r · Source: PubMed

3 AUTHORS, INCLUDING:

Vytautas Butkus
Vilnius University
25 PUBLICATIONS **234** CITATIONS

SEE PROFILE

THE JOURNAL OF PHYSICAL CHEMISTRY A

ARTICLE

pubs.acs.org/JPCA

Quantum Coherence and Disorder-Specific Effects in Simulations of 2D Optical Spectra of One-Dimensional J-aggregates

V. Butkus,[†] A. Gelzinis,[†] and L. Valkunas*[,†,‡]

[†]Department of Theoretical Physics, Faculty of Physics of Vilnius University, Sauletekio Avenue 9, build. 3, LT-10222 Vilnius, Lithuania

[‡]Center for Physical Sciences and Technology, Savanoriu Avenue 231, LT-02300 Vilnius, Lithuania

ABSTRACT: Time-resolved two-dimensional photon-echo (2D PE) spectra of linear J-aggregates containing four molecules per unit cell—a model system for a concentrated water solution of the pseudo-isocyanine dye—is theoretically considered. Analysis of a single unit cell and the full-sized aggregate is consistently carried out. Spectral features of a single unit cell are sorted out by assigning them to specific double-sided Feynman diagrams. Two different approaches of disorder are employed, the resulting differences in the spectra are discussed, and the conditions for their utilization are described. Special attention is paid to quantum coherence dynamics of a single unit cell and the full-sized J-aggregate. Possibilities of probing quantum coherences, as well as performing quantum control via two-color 2D PE spectroscopy, are discussed.

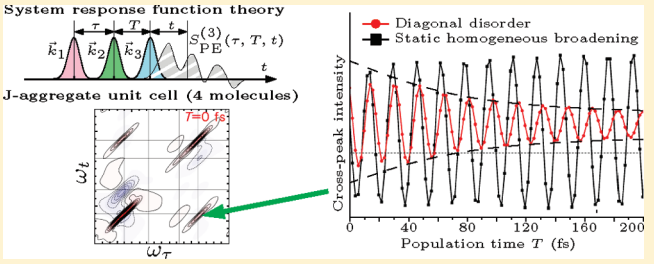

INTRODUCTION

Electronic spectra of molecular aggregates are usually attributed to Frenkel-type coherent excitons.[1] Such attribution is based on a significant shift and narrowing of the absorption band, in comparison with optical transitions of a separate molecule. This type of spectral changes in concentrated water solution of the pseudo-isocyanine (PIC) dyes was already discovered in 1936 independently by Jelley[2] and Scheibe[3] assigning the red-shifted band (the so-called "J-band") to the exciton transition in a one-dimensional molecular aggregate (the so-called "J-aggregate"). The size of the exciton coherence determines the super-radiant character of the J-band in the fluorescence spectrum.[4] The J-band in the streaming solution is polarized along the streaming direction (see, for instance, ref 5), and, thus, the transition dipole moments of the constituent molecules of the linear one-dimensional J-aggregate must have a small angle, with respect to the aggregate axis. In this case, the optical transition to the lowest exciton states dominates in the absorption spectrum, while the narrowing of its lineshape is addressed to the motional narrowing.[6,7]

During the recent decades, J-aggregates have been extensively studied both experimentally and theoretically, with the objective being to disclose their potential as nonlinear optical materials.[4,6,8−15] Strong enhancement of a nonlinear optical response of J-aggregates has been theoretically predicted.[16] Nonlinear optical techniques, such as pump−probe[8,10,12,14,15,17] and photon-echo measurements,[9,14,18,19] have enormously enriched our knowledge about the exciton dynamics, specifically disclosing the role of disorder of molecular transitions and the effects caused by multiexciton interactions. As deduced from the analysis of the exciton−exciton annihilation kinetics, the J-aggregates might contain hundreds and even thousands of constituent chromophore molecules.[8,20]

Spatial and temporal extent of exciton coherence in various molecular systems can be determined by analyzing two-dimensional photon-echo (2D PE) spectra, as has been demonstrated recently.[21,22] A molecular dimer is the simplest system where the coherent exciton feature is expected.[23] Main features of one-color and multicolor 2D PE spectra of a dimer are well-described in many theoretical studies.[24−28] The 2D PE spectroscopy was the key tool demonstrating a complex network of excitation energy transfer pathways and long-lasting coherences in a photosynthetic Fenna−Matthews−Olson (FMO) complex,[29,30] as well as in LH3 complexes from photosynthetic bacteria.[22] Recently, the 2D PE spectra have also been recorded for conjugated polymers[31] and cylindrical (bitubular) J-aggregates.[32,33] Apart from clear identification of exciton transfer between tubes, quantum coherences and population oscillations were also observed. By analyzing only the J-band of a one-dimensional J-aggregate, it was demonstrated that the 2D PE spectroscopy visualizes the intraband, heterogeneous dephasing dynamics, and the nonuniform broadening of the J-band, with respect to the main diagonal, is a signature of an interplay of population transfer and the spectral diffusion[34] and intraband coherences.[32] Analysis of the 2D spectra of the J-aggregate provides the possibility to determine the exciton delocalization size due to the J-band.[35] However, the spectrum of the PIC solution is more complex, since

Special Issue: Graham R. Fleming Festschrift

Received: August 31, 2010
Revised: January 16, 2011
Published: March 16, 2011

it contains the J-band and some other bands of shorter wavelengths, thus, indicating a more complex organization of the J-aggregate structure. On the basis of detailed analysis of the absorption and fluorescence excitation spectra, a one-dimensional model containing four molecules per unit cell was proposed.[36]

In this paper, we theoretically consider the evolution of the 2D spectra of linear J-aggregates containg four molecules per unit cell. The main emphasis is put on determination of the origin of the spectral changes caused by the unit cell and the entire aggregate. The consistent analysis is carried out by considering the third-order response at the impulsive limit of a single unit cell and a full-sized aggregate. To understand the J-aggregate-specific spectral signatures, the 2D spectra of a single unit cell are analyzed in terms of corresponding Feynman diagrams and the dominant Liouville-Space Pathways (LSPs) are revealed. The disorder-specific effects on a single unit cell are analyzed by comparing different inhomogeneous broadening implementations: inclusion of slow mode of correlation of system-environment fluctuations (static homogeneous broadening) and averaging over ensemble of random Gaussian-distributed monomer site energies (diagonal disorder). Utilization of these two approaches results in some spectral differences, the significance of which is also discussed in this paper. This study leads to predictions of the spectral behavior of full-sized aggregates. As demonstrated, the spectra of the 64-chromophore aggregate of PIC molecules reveal several differences, compared to the spectra of J-aggregates with a single molecule per unit cell.[34,35]

J-AGGREGATE MODEL

Spectral properties of J-aggregates are usually understood in terms of the Frenkel exciton theory.[4] The exciton energy spectrum and the corresponding wave functions are defined from diagonalization of the exciton Hamiltonian of a linear chain of N identical molecules:

$$\hat{H}_{\mathrm{mol}} = \sum_{m=1}^{N} (\varepsilon + \delta\varepsilon_m)|m\rangle\langle m| + \sum_{m=1}^{N}\sum_{n\neq m}^{N} J_{nm}|n\rangle\langle m| \qquad (1)$$

where ε is the excitation energy of a constituent molecule and $\delta\varepsilon_m$ is the random (inhomogeneous) Gaussian-distributed energy offset of the mth molecule, $|n\rangle$ denotes the state when the nth molecule in the aggregate is excited, and $\langle n|$ is its hermitian conjugate. Matrix elements J_{nm} denote the energies of the resonance interaction between the nth and mth molecules, which can be calculated from the structural data.

In the absence of the diagonal disorder (when $\delta\varepsilon_m \equiv 0$) and in the case of the nearest-neighbor coupling approximation (assuming that $J_{mn} = -J_0\delta_{|n-m|,1}$ with $J_0 \geq 0$), the exciton Hamiltonian defined by eq 1 can be diagonalized analytically resulting, thus, for the eigenenergies[1,4]

$$\varepsilon_j = \varepsilon - 2J_0 \cos\left(\frac{\pi j}{N+1}\right) \qquad (2)$$

and eigenfunctions $|e_j\rangle = \sum_n \psi_{jn}|n\rangle$, where

$$\psi_{jn} = \sqrt{\frac{2}{N+1}} \sin\left(\frac{\pi jn}{N+1}\right) \qquad (3)$$

Quantum numbers $j = 1, ..., N$ enumerate the one-exciton states. The transition dipole moments corresponding to each exciton state are defined, giving the dipole strength for a particular exciton state, as follows:

$$(\mu_j)^2 = \left(\frac{2{\mu_0}^2}{N+1}\right) \cot^2\left[\frac{\pi j}{2(N+1)}\right] \qquad (4)$$

for odd j and

$$(\mu_j)^2 = 0 \qquad (5)$$

for even j, where μ_0 denominates the transition dipole moment of a constituent molecule from the aggregate. Thus, the dipole strength of the lowest energy state ($j = 1$), which is red-shifted, in comparison with the molecular transition, in accord with eq 2, is significantly higher than that of the others and contains more than 80% of the total oscillator strength. $N(N-1)/2$ two-exciton states form a manifold of higher-energy states. The corresponding eigenenergies and transition dipole moments can be obtained from a two-excitonic Hamiltonian analogously.[21] Further in this paper we will use subscripts e_j and f_k to indicate one-exciton ($j = 1, \ldots, N$) and two-exciton ($k = 1, \ldots, N(N-1)/2$) states, respectively.

The spectral inhomogeneity of the molecular transitions caused by the diagonal disorder, i.e., when $\delta\varepsilon_m \neq 0$, essentially perturbs this simplified picture, which should be perceptible in the 2D spectra.[34,35] To extract the possible manifestation of the structural organization and inhomogeneity, numerical diagonalization of the exciton Hamiltonian beyond the nearest-neighbor approximation will be used for further characterization of the exciton spectrum.

The absorption spectrum of PIC aggregates contains three well-resolved bands: the J-band at 576.5 nm and two weak bands at 536 and 499 nm. Having the background absorption excluded, the intensities of the absorption between these bands are distributed as 54.7%, 11.4%, and 33.9% of the total oscillator strength, respectively, at 77 K. Although the origin of the J-band is attributed to the most intensive long-wavelength excitonic transition, the origin of the other two peaks is still questionable. It has been proposed[36] that all bands are caused by the purely excitonic transitions. According to this model, the unit cell of the aggregate consists of four PIC molecules and, within the dipole approximation, the transition dipoles in the unit cell are of the following orientation: (μ_x, μ_y, μ_z), $(-\mu_x, -\mu_y, \mu_z)$, $(\mu_x, -\mu_y, \mu_z)$, and $(-\mu_x, \mu_y, \mu_z)$, where $\vec{\mu} = (\mu_x, \mu_y, \mu_z) = (0.581, 0.338, 0.738)$. These transition dipole moments cause the average value of the coupling constant between the nearest neighbors J_0 being equal to -1.43 in units of $|\vec{\mu}|^2/(r_{12})^3$, where r_{12} is the translation vector norm. An experimentally observed exciton bandwidth is achieved by setting $|\vec{\mu}|^2/(r_{12})^3$ to reach $J_0 = 600$ cm^{-1}. To verify this attribution, we will consider the 2D spectra of such aggregate.

SIMULATION RESULTS

Simulation Parameters. An experimental scheme of 2D PE spectroscopy is presented in Figure 1a. Three wave vectors of ultrashort laser pulses exciting the sample at times τ_1, τ_2, and τ_3 are denoted as $\vec{k}_1$, $\vec{k}_2$, and $\vec{k}_3$, respectively. The induced third-order polarization within the sample is the source of the radiated electric field. Because the phase-matching condition is assured, the measured intensity is proportional to the squared absolute value of polarization. The PE signal (polarization) is generated in the direction $\vec{k}_{\mathrm{PE}} = -\vec{k}_1 + \vec{k}_2 + \vec{k}_3$ and detected as a superposition with a heterodyne pulse $\vec{k}_{\mathrm{h}}$. The heterodyne pulse does not contribute to the signal in the detection direction; therefore, it is

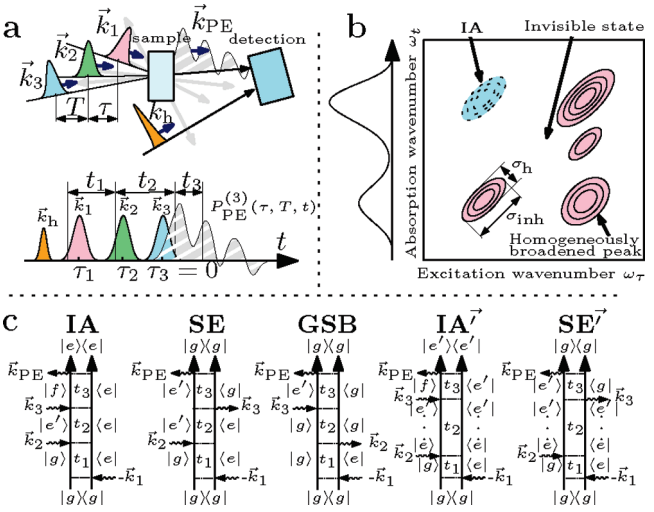

Figure 1. (a) 2D PE experimental scheme and definitions of variables: τ_1, τ_2, and τ_3 are the times of three laser pulses exciting the sample, whereas t_1, t_2, and t_3 are the time variables for the system response function (see text for details). (b) Example of 2D spectrogram with inhomogeneous and homogeneous lineshape widths identified (σ_{inh} and σ_h, respectively). (c) Total set of double-sided Feynman diagrams for the $\vec{k}_{PE} = -\vec{k}_1 + \vec{k}_2 + \vec{k}_3$ experimental direction at the impulsive limit.

not considered in calculations. Since the absolute interaction time is irrelevant (because of the system being in thermal equilibrium before the first interaction) the PE signal can be characterized as a three-variable function of positive delay times between successive laser pulses $\tau \equiv \tau_2 - \tau_1$ and $T \equiv \tau_3 - \tau_2$ and the detection time t. The Fourier-transformed function of variables $\tau \rightarrow \omega_\tau$ and $t \rightarrow \omega_t$ is plotted as a two-dimensional spectrogram (Figure 1b). Such signal is denoted as "rephasing", since the dephasing in the system is opposite after the first and third interaction and at $\tau = t$, the inhomogeneous broadening is eliminated. In spectra, it is observed as peak elongation along the main diagonal. Similarly, signal, generated at non-PE direction $+\vec{k}_1 - \vec{k}_2 + \vec{k}_3$, is denoted as nonrephasing. The inhomogeneous contribution is not eliminated and the peak lineshapes are oriented in an antidiagonal direction. The same signal would be measured in the PE direction $\vec{k}_{PE}$ if the first and second pulses were switched (assuming $\tau < 0$). The sum of rephasing and nonrephasing signals gives the total, pump−probe-like spectra.[26,27,37] Usually, the real part of the total or rephasing spectra is used for interpretation.

To simulate the third-order polarization for 2D spectra calculations, we use the system response function theory considering the field-matter interaction perturbatively, in terms of the time-dependent density operator.[37,38] The third-order polarization is obtained as a triple convolution of the system response function $S^{(3)}(t_3, t_2, t_1)$ and the sample-exciting electric field

$$P_{PE}^{(3)}(\tau, T, t) = \int_0^\infty dt_3 \int_0^\infty dt_2 \int_0^\infty dt_1 S^{(3)}(t_3, t_2, t_1) \times E(\vec{r}, t - t_3) E(\vec{r}, t - t_3 - t_2) \times E(\vec{r}, t - t_3 - t_2 - t_1) \quad (6)$$

The electric field function is composed of three ultrashort laser pulses, propagating in directions $\vec{k}_1$, $\vec{k}_2$, and $\vec{k}_3$:

$$E(\vec{r}, t) = \sum_{j=1}^{3} \mathcal{E}_j(t - \tau_j) \exp(-i\omega_j(t - \tau_j) + i\phi_j + i\vec{k}_j\vec{r}) + c.c. \quad (7)$$

Here, $\mathcal{E}_j$, ω_j, and ϕ_j are the envelope, carrier frequency, and phase of the jth pulse, respectively.

The total system response is resolved as several oscillating patterns corresponding to LSPs. The complete set of double-sided Feynman diagrams, representing these pathways, is reduced to five diagrams, depicted in Figure 1c, in case of $\mathcal{E}_j(t) \equiv \delta(t)$ (the so-called "impulsive limit") is used. Using a second-order cumulant-expansion technique, the shapes of spectral elements of the oscillating terms in the frequency domain are determined by summarizing the time-dependent lineshape functions, which are calculated using the classically defined spectral density function $\mathcal{C}''(\omega)$ of the bath fluctuations:

$$g(t) \equiv \frac{1}{2\pi} \int_{-\infty}^{\infty} d\omega \frac{C''(\omega)}{\omega^2} \left[(1 - \cos\omega t) \coth\left(\frac{\omega}{2\theta}\right) + i(\sin\omega t - \omega t) \right] \quad (8)$$

The entire quantum-mechanical correlation function involving effects of irreversible exciton relaxation is constructed from the classically defined odd part, $\mathcal{C}''(\omega)$, invoking a fluctuation−dissipation theorem and the detailed-balance condition.[38,39] In our simulations, the environment-induced fluctuations are described using the corresponding spectral density of the overdamped Brownian oscillator (BO), which is characterized by the relaxation rate Λ and the coupling strength λ. The corresponding classical spectral density for one mode of phonon-bath fluctuations is as follows:[40]

$$\mathcal{C}''(\omega) = 2\lambda\Lambda \frac{\omega}{\omega^2 + \Lambda^2} \quad (9)$$

It represents the energy correlations of the electronic subsystem, which are strongly overdamped by the phonon-bath motion. The molecules are assumed to have their own linearly coupled harmonic baths and the phonon-induced dynamics at different sites are not correlated. At the high-temperature limit ($\theta \gg \Lambda$, where θ is the thermal energy), the integration can be performed analytically. It results in the lineshape function

$$g(t) = \frac{\lambda}{\Lambda}\left(\frac{2\theta}{\Lambda} - i\right)(e^{-\Lambda t} + \Lambda t - 1) \quad (10)$$

The relaxation rates are calculated using the traditional Redfield theory:

$$K_{ab} = \mathrm{Re}\eta_{ab}\mathcal{C}''(\omega_{ab})\left[\coth\left(\frac{\omega_{ab}}{2\theta}\right) - 1\right] \quad (11)$$

Here, η_{ab} is the wave function overlap contribution ($\eta_{ab} = \sum_{n,m}\psi_{am}{}^2\psi_{bn}{}^2$) and ω_{ab} is an energy gap ($\omega_{ab} = \varepsilon_a - \varepsilon_b$). The relaxation rates define electronic population state transfer during interval t_2, while the coherent state dynamics during intervals t_1 and t_3 are described by thermal-bath-induced pure dephasing.

Two additive modes of overdamped BO spectral density (eq 9) can be considered: $\mathcal{C}''_F(\omega)$ corresponds to the fast fluctuations of a phonon bath and contributes to a homogeneous broadening of spectral lineshapes, and $\mathcal{C}''_S(\omega)$ simulates inhomogeneous broadening of the spectra.[40,41] These modes are denoted as "fast" and "slow", respectively. Since the inhomogeneous lineshape widths of

a

	Dipole moment	Value	Diagram	Peak position (ω_τ, ω_t)
A	$\langle\lvert\vec{\mu}_{ge_1}\rvert^2\lvert\vec{\mu}_{e_1f_1}\rvert^2\rangle$	1.22	IA_p	ε_{e_1}, $\varepsilon_{e_2} - 51\,cm^{-1}$
B	$\langle\lvert\vec{\mu}_{ge_1}\rvert^4\rangle$	0.90	GSB, SE_p	ε_{e_1}, ε_{e_1}
C	$\langle\lvert\vec{\mu}_{ge_4}\rvert^2\lvert\vec{\mu}_{e_4f_6}\rvert^2\rangle$	0.44	$IA_p{}^a$	ε_{e_4}, $\varepsilon_{e_3} - 16\,cm^{-1}$
D	$\langle\lvert\vec{\mu}_{ge_4}\rvert^4\rangle$	0.34	GSB, $SE_p{}^a$	ε_{e_4}, ε_{e_4}
E	$\langle\lvert\vec{\mu}_{ge_4}\rvert^2\lvert\vec{\mu}_{e_1f_1}\rvert^2\rangle$	0.25	IA'	ε_{e_4}, $\varepsilon_{e_2} - 51\,cm^{-1}$
F	$\langle\lvert\vec{\mu}_{ge_1}\rvert^2\lvert\vec{\mu}_{ge_4}\rvert^2\rangle$	0.18	GSB, SE_c	ε_{e_1}, ε_{e_4}
G	$\langle\lvert\vec{\mu}_{ge_4}\rvert^2\lvert\vec{\mu}_{ge_1}\rvert^2\rangle$	0.18	GSB, SE_c, SE'	ε_{e_4}, ε_{e_1}
H	$\langle\lvert\vec{\mu}_{ge_4}\rvert^2\lvert\vec{\mu}_{e_1f_2}\rvert^2\rangle$	0.17	IA'	ε_{e_4}, $\varepsilon_{e_3} + 41\,cm^{-1}$
I	$\langle\lvert\vec{\mu}_{ge_3}\rvert^2\lvert\vec{\mu}_{e_1f_1}\rvert^2\rangle$	0.13	IA'	ε_{e_3}, $\varepsilon_{e_2} - 51\,cm^{-1}$
J	$\langle\lvert\vec{\mu}_{ge_1}\rvert^2\lvert\vec{\mu}_{ge_3}\rvert^2\rangle$	0.09	GSB, SE_c	ε_{e_1}, ε_{e_3}
K	$\langle\lvert\vec{\mu}_{ge_3}\rvert^2\lvert\vec{\mu}_{ge_1}\rvert^2\rangle$	0.09	GSB, SE_c, SE'	ε_{e_3}, ε_{e_1}
L	$\langle\lvert\vec{\mu}_{ge_4}\rvert^2\lvert\vec{\mu}_{e_4f_5}\rvert^2\rangle$	0.08	$IA_p{}^a$	ε_{e_4}, $\varepsilon_{e_2} - 41\,cm^{-1}$
M	$\langle\lvert\vec{\mu}_{ge_1}\rvert^2\lvert\vec{\mu}_{e_1f_2}\rvert^2\rangle$	0.07	IA_p	ε_{e_1}, $\varepsilon_{e_3} + 41\,cm^{-1}$
N	$\langle\lvert\vec{\mu}_{ge_3}\rvert^4\rangle$	0.05	GSB, $SE_p{}^a$	ε_{e_3}, ε_{e_3}

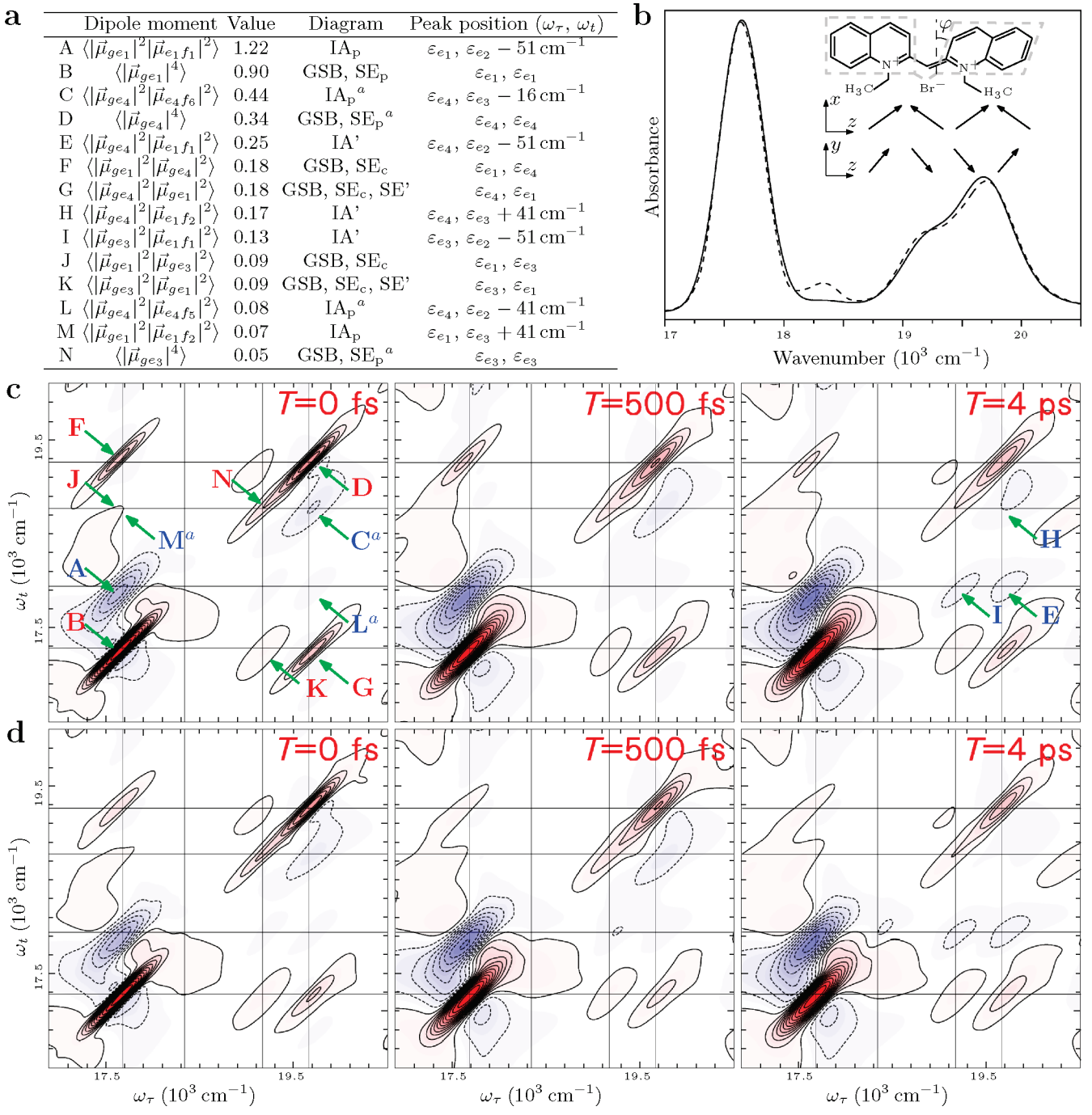

Figure 2. (a) Orientationally averaged dipole moment products, their intensities, corresponding Feynman diagrams, and approximate peak positions in the 2D spectra. Superscript *a* denotes response contributions, decreasing in the course of *T*, because of the decay of population transfer (or survival probability). Calculated absorption and 2D spectra by taking into account the diagonal disorder by averaging the spectra over 1000 realizations with Gaussian-distributed diagonal disorder with a standard deviation of $\sigma_D = 300\ cm^{-1}$ and choosing $J_0 = 600\ cm^{-1}$ (dashed line in panel b and row c); a static inhomogeneous broadening approach is used, assuming the following parameters for the "slow" mode of phonon-bath fluctuations: $\Lambda_S{}^{-1} = 200$ ps and $\lambda_S = 1000\ cm^{-1}$, and also choosing $J_0 = 625\ cm^{-1}$ (solid line in panel b and row d). Spectra shown in panels c and d correspond to delay times of $T =$ 0, 0.5, and 4 ps; contours are plotted on the arcsinh scale.

all the system's molecules are affected in the same way (i.e., homogeneously), we are referring to this simulation regime as the "static homogeneous broadening" throughout this paper. The other possible way to take the inhomogeneity into consideration is to add a random Gaussian-distributed disorder of monomer transition energies $\delta\varepsilon_m$ (diagonal disorder) and use only the "fast" mode for the overdamped BO spectral density. In that case, averaging over many 2D spectra simulations must be done. Both methods are compared to analyze the possible differences in the 2D and absorption spectra.

Simulation parameters were defined by fitting the simulated absorption spectra of a full-sized aggregate to the experimentally

dx.doi.org/10.1021/jp108291r |J. Phys. Chem. A 2011, 115, 3876–3885

obtained absorption spectrum of the PIC J-aggregate using spatial configuration of molecules, as described previously. In simulations, it was done using a diagonal disorder of chromophore energies and averaging over 1000 realizations with a different number of chromophores. Overdamped BO parameters of the "fast" mode Λ_F^{-1} = 200 fs and λ_F = 125 cm^{-1} and population lifetimes of τ_{536} = 77 fs and τ_{499} = 48 fs to obtain the correct broadening of the bands at 536 and 499 nm, respectively, were used in calculations. A standard deviation $\sigma_D = 0.1 \times J_0$ = 60 cm^{-1} of the Gaussian-distributed random chromophore energy was chosen to fit the width of the J-band. The absorption spectra do not show any essential changes for large aggregates when $N > 64$; therefore, the 64-chromophore J-aggregate (16 unit cells) is denoted as a "full-sized" aggregate throughout this article.

Single Unit Cell. First let us consider a single unit cell only, which is a complex of four excitonically coupled molecules. This consideration would help us to distinguish the spectral characteristics of a unit cell from those corresponding to the entire aggregate in later analysis of the full-sized aggregate. Moreover, four excitonically coupled molecules constitute a larger system than a molecular dimer, which is usually considered as an archetype model of an excitonically coupled system.[24,28,40] Thus, comparison of the 2D spectra for the unit cell and the 2D spectra of the dimer is useful to describe the spectral variability due to the increasing amount of molecules in the aggregate.

The calculated absorption spectrum of a single unit cell at 77 K is presented in Figure 2b. It is noteworthy that the enhancement of the longest wavelength absorption band corresponding to the transition into the lowest exciton state is already perceptible. Additional two overlapping peaks are positioned on the shorter wavelength part of the spectrum, while the optically forbidden transition is observed at 18 340 cm^{-1}.

It is convenient to identify separate spectral elements in the 2D spectra, attributing them to corresponding Feynman diagrams (presented in Figure 1c) by analyzing the highest values of orientationally averaged dipole moments, as given in Figure 2a. Here, selected elements constitute 87% of the total third-order response signal at the initial time $T = 0$, while the elements responsible for peaks outside the one-exciton band region are not included. The corresponding spectral signatures are identified in the 2D spectra shown in Figure 2c.

The positive peaks in the 2D spectra correspond to the ground-state bleaching (GSB) and the stimulated emission (SE). In the GSB diagram, only the ground state is active during T. Therefore, the corresponding contribution reflects the dephasing process only and the spectral evolution defined by this diagram does not demonstrate any significant changes in both diagonal and off-diagonal peaks. In contrast, the processes reflecting the population transfer manifest themselves in the SE diagram. The diagonal element in the highest energy state decays with T, because of unambiguous population relaxation to the lowest exciton state from the higher states of the one-exciton band (peak D in Figure 2c). The cross-peaks are also defined by the coherent SE (SE_c) diagram (see F, G, J, and K in Figure 2c). Additionally, they show oscillating dynamics in the course of T, reflecting the coherence beats of the density matrix for the one-exciton states. Positive peaks below the diagonal (G and K) get broader with T. This indicates the additional dephasing caused by population transfer in the stimulated emission diagram (SE′).

Negative cross-peaks at the initial times reflect the induced absorption pathways (IA). An intensive off-diagonal element at $\omega_\tau = \varepsilon_{e_1}$, $\omega_t \approx \varepsilon_{e_2}$ (see A in Figure 2) appears because of the $|f_1\rangle\langle e_1|$ coherence created after the third interaction. The peak appears by $\varepsilon_{e_2} - (\varepsilon_{f_2} - \varepsilon_{e_1}) \approx 51$ cm^{-1} lower than the eigenenergy ε_{e_2}. Similarly, when population $|e_4\rangle\langle e_4|$ evolves to the $|f_6\rangle\langle e_4|$ coherence, as a result of the light-induced transition, the peak at $\omega_\tau = \varepsilon_4$, $\omega_t = \varepsilon_{f_6} - \varepsilon_{e_4} \approx \varepsilon_{e_3} - 16$ cm^{-1} emerges (C in Figure 2c). These diagrams contain population state survival probabilities over the course of T, which decays rapidly for all states except $|e_1\rangle\langle e_1|$. Therefore, the peak at $\omega_\tau = \varepsilon_4$, $\omega_t \approx \varepsilon_{e_3}$, as well as other elements for $\omega_\tau \neq \varepsilon_1$, vanish at longer delay times (see C and L in Figure 2). The collateral process of the population transfer (IA′) is also responsible for negative peaks indicated as E, H, and I in Figure 2. However, they are observed at the same position as the decaying cross-peaks corresponding to IA. The decay of IA and the growth of IA′ proceed on different time scales. The dominant input from the population transfer diagram denotes the generation of populations $|e_3\rangle\langle e_3|$ and $|e_4\rangle\langle e_4|$ (light-induced transition to the second excited state is forbidden) with a subsequent relaxation to the $|e_1\rangle\langle e_1|$ state in the course of T. Peak positions with respect to the ω_t-axis indicate coherences with two-exciton states, $|f_j\rangle\langle e_1|$.

Comparing the 2D spectra of the system of four molecules with an excitonically coupled dimer, some principal differences are evident. In the dimer system, the IA and IA′ contributions act mainly on the upper left cross-peak, as well as SE and GSB diagrams. Depending on the spatial configuration of chromophore dipoles and the resonant coupling strength, this superposition might even result in the cancellation of GSB and IA contributions and a zero-intensity cross-peak. In the system of four excitonically coupled molecules, the most intensive IA contribution is isolated from intensive GSB contributions and can be clearly identified as a negative peak above the lowest diagonal element. It is similar to IA′ contributions, which act at the same ω_t frequencies as IA. The cross-peaks from the SE, SE′, and GSB diagrams correspond to the coherences of one-exciton energies as in the case of the dimer system. Therefore, with certain parameters, positive cross-peaks might create the dimer-like spectra, but the IA contributions will be displaced differently than for the excitonically coupled dimer.

Simulation of Inhomogeneous Broadening of the Unit Cell. The disorder of molecular systems can make a significant impact in their spectroscopic features. In simulations, the offset term $\delta\varepsilon_m$ in the molecular Hamiltonian (eq 1) determining the diagonal disorder should be taken into accout. Gaussian randomness of the transition dipole moment orientations, referred to as off-diagonal disorder due to variability of the off-diagonal elements of the Hamiltonian, can also be considered. Both types of disorder tend toward making localization of the exciton states more pronounced at the band edges.[4] If the delocalization length at the band edges is smaller than the aggregate length, spectroscopic properties do not change with further enlargement of the aggregate size, defined by the amount of its constituents N.

To demonstrate the principal effects caused by the disorder, usually the diagonal disorder is taken into consideration. To highlight disorder-specific effects in the system of a single unit cell, a deliberately larger amount of diagonal disorder with σ_D = 300 cm^{-1} is assumed. Two different approaches for simulations of the system inhomogeneity are used: (i) inclusion of a "slow" mode of the overdamped BO into the spectral density (eq 9) and (ii) averaging over an ensemble of aggregates with random Gaussian-distributed chromophore energies $\varepsilon + \delta\varepsilon_m$ in the Frenkel exciton Hamiltonian. Using the first approach, the

broadening of the lineshapes is achieved by a direct modification of the lineshape functions and the system eigenstates are not affected.[40] Although individual chromophores might be assigned to different parameters of the spectral density, in the case of the uniform "slow" mode, the oscillator strengths and positions of the absorption peaks of the exciton transitions change in the same way. This approach is denoted as a static homogeneous broadening. The other method is a straightforward simulation of the disorder in the system, averaging over many realizations. In this case, the diagonalization of the molecular Hamiltonian, as well as calculation of the optical transitions, must be carried out for every realization. This can result in significant changes in the absorption spectra, such as an uprise of an optically forbidden absorption band at 18 340 cm^{-1} (Figure 2b), while simulating the absorption spectrum with a static homogeneous broadening, this absorption band was absent, denoting forbiddeness of the optical transition to the second excitonic state. The diagonal disorder also expands the spectral region corresponding to the excitonic transitions. Therefore, the resonant coupling constant was tuned and $J_0 = 625$ cm^{-1} was chosen for calculations with the "slow" mode of the BO to fit the absorption spectrum.

The real parts of the rephasing 2D spectra, calculated using both methods accounting for the inhomogeneous broadening, are depicted in Figures 2c and 2d. Although different approaches to the inhomogeneous broadening give qualitative differences in the absorption spectrum, no essential variations of the 2D spectra are distinguished. The method based on the diagonal disorder does not give any evident increase in the diagonal elements of the spectra corresponding to the second one-exciton state. This is because the peak heights in the 2D spectra are proportional to the fourth order of the dipole moments of corresponding optical transitions. No significant changes in nonrephasing spectra were also observed (not shown).

J-band Region of Full-Sized J-aggregates. Let us now consider the 2D spectra of the J-aggregate containing 64 monomers ($N = 64$), i.e., the aggregate with 16 unit cells. Absorption spectra simulated for larger aggregates did not contain any notable differences, which means that the exciton coherence length in the aggregate of such size and for the disorder value chosen in our simulations is shorter than the aggregate size, and further elongation of the aggregate would not change its density of states. Therefore, we restrict our consideration to the aggregate containing 64 monomers and denote it as the full-sized aggregate.

Spectra of the full-sized J-aggregates were calculated using the same two approaches to the inhomogeneous broadening as was done by analyzing the spectra of the unit cell. Simulations with diagonal disorder were carried out by averaging the Gaussian distribution of the $\delta\varepsilon_m$ value (for $m = 1, ..., 64$) over 1000 realizations with the standard deviation $\sigma_D = 60$ $cm^{-1} = 0.1J_0$. Parameters of the "slow" mode of the overdamped BO spectral density $\lambda_S = 120$ cm^{-1} and $\Lambda_S^{-1} = 200$ ps were chosen by fitting with absorption spectra, obtained using the diagonal disorder approach. The resonant coupling value is assumed to be equal to $J_0 = 605$ cm^{-1}. Absorption spectra simulations using both models are presented in Figure 3a. It is important to mention that the optical transitions to the homogeneously broadened higher-energy excitonic states are well-resolved, which is not the case for the J-aggregates containing one molecule per unit cell.

Two-dimensional (2D) spectra of the J-band of full-sized J-aggregates with a single molecule per unit cell have been reported recently.[34,35] The J-band in the 2D spectra is related

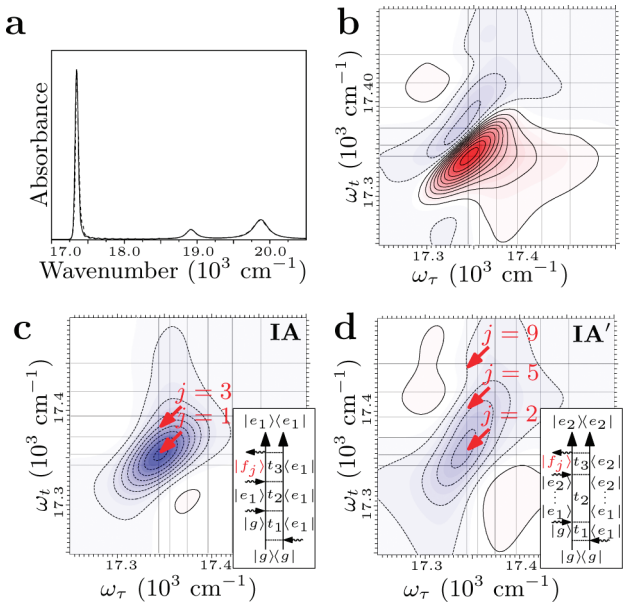

Figure 3. (a) Absorption spectra of the J-aggregate containing 64 monomers ($N = 64$) calculated by means of the numerical averaging over 1000 realizations and assuming a Gaussian distribution of the diagonal disorder with the standard deviation $\sigma_D = 60$ cm^{-1} (dashed line) and by assuming a static inhomogeneous broadening (solid line), (b) Total 2D spectrum of this aggregate in the static homogeneous broadening regime at $T = 500$ fs. (c) IA contributions of this aggregate. (d) Population transfer IA′ contributions of this aggregate.

to a superposition of a few different LSPs. In the real part of the total 2D spectrum, the main positive peak is formed by the GSB and SE pathways. Negative peaks above this region appear because of the induced absorption with or without the population transfer (IA′ or IA, respectively). Induced absorption reveals coupling to the two-exciton states, the most intensive of which is positioned at $\omega_t = \varepsilon_{f_1} - \varepsilon_{e_1} = \varepsilon_{e_2}$. Population transfer pathways produce negative elements in the vicinity of the J-band, because of the fact that energetic separation of the one-exciton levels at the lower edge of the excitonic band is comparable with the thermal energy, $\omega_{e_2e_1} \approx \theta$. Thus, the thermalization of one-exciton state populations causes the upward population transfer. Such a type of transfer is never achievable in smaller aggregates, where the density of states is small and the energy gap between exciton states is large, in comparison to the thermal energy, $\omega_{e_2e_1} > \theta$. The population transfer contribution is negligible at short delay times, while the induced absorption diagram decays with T on a different time scale, compared to the population transfer.

Such superposition of different LSPs in the full-sized J-aggregates results in complicated 2D spectra in the vicinity of the J-band at lower temperatures. The main positive peak is distorted by negative contributions and by measuring this distortion (antidiagonal width) of the J-band in the 2D spectra, it is possible to distinguish the population transfer contribution.[34]

Since more than one delocalized exciton state determines the formation of the J-band, the intraband cross-peaks are also expected. Such electronic coherences result in off-diagonal intraband oscillations.[35] The dominant cross-peak is addressed to the $|e_1\rangle\langle e_3|$ coherence, and it is expected to be observed in measurements with suppressed homogeneous broadening as the nonsymmetrical wing in the main positive peak of the J-band.

Spectra of a full-sized J-aggregate with four molecules per unit cell have very similar features, compared to the spectra of aggregates with one molecule per unit cell (see Figure 3b). The main peak is nonsymmetric, with a wing elongated along ω_τ, witnessing the $|e_1\rangle\langle e_3|$ one-exciton coherence. This coherent contribution is oscillating with intraband frequency and the main peak is "breathing" in the course of T. There are two dominant induced absorption pathways (Figure 3c) maintaining coherences of the most delocalized one- and two-exciton states, $|f_1\rangle\langle e_1|$ and $|f_3\rangle\langle e_1|$, respectively.

Population transfer manifests itself in three most intensive pathways in the vicinity of the J-band. In all of them, the population is transferred energetically upward from $|e_1\rangle\langle e_1|$ to $|e_2\rangle\langle e_2|$ during T and the $|f_2\rangle\langle e_2|$, $|f_5\rangle\langle e_2|$, and $|f_9\rangle\langle e_2|$ coherences are created after interaction with the third laser pulse. Positions of spectral elements reflecting those pathways are indicated by arrows in Figures 3c and 3d. The distance between adjacent exciton states is $\varepsilon_{e_2} - \varepsilon_{e_1} \approx 0.2\theta$ at the lower edge of a one-exciton manifold; therefore, the thermalization of the populated states essentialy differs from the result corresponding to the unit cell. In a single unit cell, $\varepsilon_{e_2} - \varepsilon_{e_1} \approx 11\theta$ holds; thus, the downward population transfer dominates (peaks I and E in Figure 2).

DISCUSSION

As demonstrated by modeling the 2D spectra of a four-molecule unit cell of the J-aggregate, the origin of diagonal elements and cross-peaks can be evidently attributed to specific double-sided Feynman diagrams. The diagrams corresponding to the induced absorption contribution result in the differences from the 2D spectra of the dimer. It was also revealed that the inhomogeneous distrubution can be taken into account as a static homogeneous broadening, which essentially reduces the computational time, in comparison with calculations, by taking the diagonal disorder into account via the ensemble averaging procedure. However, this assumption must be more carefully analyzed by considering the problem of coherence dynamics.

Indeed, the electronic coherence of the lowest and highest eigenstates, $|e_1\rangle\langle e_4|$, demonstrates different dynamics when different approaches of inhomogeneous broadening are utilized. The differences might be distinguished from the delay time (T) dependence of the intensity of the corresponding cross-peak $A_{4,1}$ positioned at $(\omega_\tau, \omega_t) = (\varepsilon_{e_4}, \varepsilon_{e_1})$. Using the diagonal disorder approach, the maxima of the $A_{4,1}$ cross-peak, as well as the opposite peak above the diagonal, are observed to be less intensive than the peaks obtained in the static homogeneous broadening limit at a longer delay time T (see Figure 2). The intensity of this cross-peak should oscillate with the frequency related to the entire excitonic bandwidth, $\Delta_e^{(4)}$. The corresponding dynamics, as a function of the normalized cross-peak intensity, is presented in Figure 4a. As demonstrated, the diagonal disorder scheme provides a more rapid decay of electronic coherence oscillations, in contrast to the long-lasting coherence that follows from the static homogeneous broadening simulations. In the limit of the diagonal disorder, the recorded cross-peak intensity represents a statistical average of various coherences. Thus, the pathways giving oscillations of slightly different frequencies and phases are summarized and provide the total deteriorated signal. In terms of the formation of spectral elements, the decrease of intensities of the cross-peaks in the diagonal disorder simulation regime can be depicted as a destructive interference of positive and negative parts of the cross-peak lineshapes. Similarly, the inhomogeneous broadening, "bleaches" the nonrephasing contribution in the total 2D spectra.

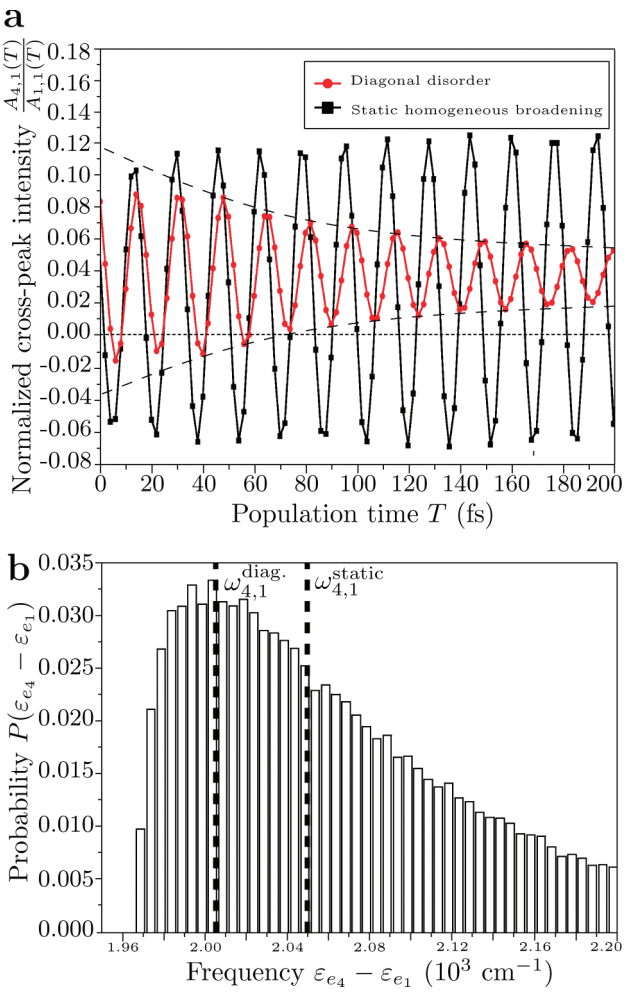

Figure 4. Oscillations of the cross-peak at $(\omega_\tau, \omega_t) = (\varepsilon_{e_4}, \varepsilon_{e_1})$ for a single unit cell at different implementations of inhomogeneous broadening (upper panel). The intensities were obtained for the impulsive-limit conditions, using the same parameters as in Figure 2. The distribution histogram (probability) of the energy gap $\varepsilon_{e_4} - \varepsilon_{e_1}$, calculated using 50000 realizations with the diagonal disorder (lower panel).

Cross-peaks also demonstrate oscillations of slightly different frequencies in the two regimes. In the case of the diagonal disorder, the cross-peak oscillation frequency corresponds to the full width of the excitonic band, $\omega_{4,1}^{\text{diag}} = \Delta_e^{(4)}$, and for the static homogeneous broadening limit this frequency is higher, $\omega_{4,1}^{\text{static}} = (\varepsilon_{e_4} - \varepsilon_{e_1})_{\delta\varepsilon_m=0} = \Delta_e^{(4)} + 46$ cm^{-1}. Since the absorption spectrum simulations provide perfect agreement of the experimentally observed positions of the optical transition bands, this frequency shift of the cross-peak oscillations can only be explained by correlation of one-exciton energies ε_{e_4} and ε_{e_1} in the presence of the diagonal disorder. The measured oscillation frequency is the expectational value of the interstate transition frequency $\langle\varepsilon_{e_4} - \varepsilon_{e_1}\rangle_{\delta\varepsilon_m}$. The distribution histogram of the energy difference $\varepsilon_{e_4} - \varepsilon_{e_1}$ is presented in Figure 4b. The distribution has its maximum exactly at $\omega_{4,1}^{\text{diag}}$. The oscillation frequency measured in the system without disorder ($\omega_{4,1}^{\text{fast}}$) is lower than that in the

other two regimes, since the exciton band is narrower, because of a lower value of the resonant coupling constant.

Considering the 2D spectra of the full-sized J-aggregates, the super-radiant J-band and the spectral region reflecting the coherence dynamics outside the J-band are of special interest. The presence of four molecules per unit cell is an important issue while analyzing these two spectral regions separately. According to our simulation results, the spectra of the J-band only do not provide any information regarding the constitution of a unit cell; the obtained spectra are similar to the spectra of J-aggregates with one molecule per unit cell.[34,35] However, the aggregates with 4 molecules per unit cell maintain coherences outside the J-band between the lowest exciton and the excitons of higher energies.

Thus, let us discuss the electronic coherence between the most delocalized one-exciton states at both ends of the one-exciton band of a full-sized ($N = 64$) J-aggregate, denoted as $|e_1\rangle$ and $|e_{64}\rangle$. The corresponding coherence $|e_1\rangle\langle e_{64}|$ would demonstrate quantum beats of frequency of the one-exciton bandwidth $\omega_{64,1} = \Delta_e^{(64)}$. For our model of the PIC J-aggregate, we get $\Delta_e^{(64)} \approx 1.2\Delta_e^{(4)}$. To excite all transitions in the one-exciton band, laser pulses at least as short as $\sigma_t \approx 4$ fs must be used. However, preparation of such short and phase-stabilized laser pulses experimentally is not possible. Therefore, the two-color (2C) 2D technique could be the other approach used for discrimination between the LSPs. As it was already demonstrated for the dimer systems, this approach gives the possibility of extracting individual pathways by utilizing narrow-bandwidth laser pulses of different wavelengths.[23,28,42] This technique also demonstrates the promises in performing Quantum Process Tomography (QPT) of the density matrix elements.[43] Wavelenghts of three consecutive laser pulses, (ω_1, ω_2, ω_3), can be tuned to trigger certain resonances in the excitonic system, thus selecting the different LSPs, addressed to different Feynman diagrams. However, the effectiveness of this technique is limited by the density of states in a particular spectral region. Although it is possible to extract all individual spectral elements in an excitonic dimer and reconstruct the full spectrum using narrow-bandwidth simulations, such a clear separation of individual pathways, however, is impossible in the J-band region of full-sized J-aggregates, since many different diagrams remain active in a small spectral region.

However, it is not the case for isolated cross-peaks of the full-sized aggregates. By recording the intensity of the cross-peak positioned at $(\omega_\tau, \omega_t) = (\varepsilon_{e_{64}}, \varepsilon_{e_1})$ as a function of $A_{64,1}(T)$ and using δ-shaped laser pulses, two dominating pathways are probed in the same position. Oscillations are produced by the stimulated emission, maintaining $|e_1\rangle\langle e_{64}|$ coherence, and a pathway of population transfer from the highest one-exciton state to the lowest state manifests itself in an increasing bias intensity over T. For the resonant selection of the corresponding SE diagram, laser pulse wavelength configuration $\{\omega_1, \omega_2, \omega_3\} = \{\varepsilon_{e_{64}}, \varepsilon_{e_1}, \varepsilon_{e_{64}}\}$ is used and the pulse lengths are varied from $\sigma_t = 4$ fs to $\sigma_t = 50$ fs. From the cross-peak intensity function (Figure 5), it is obvious that no population transfer pathways are active in this scheme, since the function has zero offset. They are triggered only in simulations with $\sigma_t < 4$ fs (not shown). The $A_{64,1}(T)$ function does not demonstrate any significant changes, even if the pulse length is longer than $\sigma_t = 50$ fs. In Figure 5, it is also evident that coherence does not decay as fast as expected. This is due to the utilization of static homogeneous broadening approach, as discussed previously for a single unit cell.

To demonstrate the sensitivity of the 2C 2D spectra to the off-resonant laser pulses, let us consider the following dominating

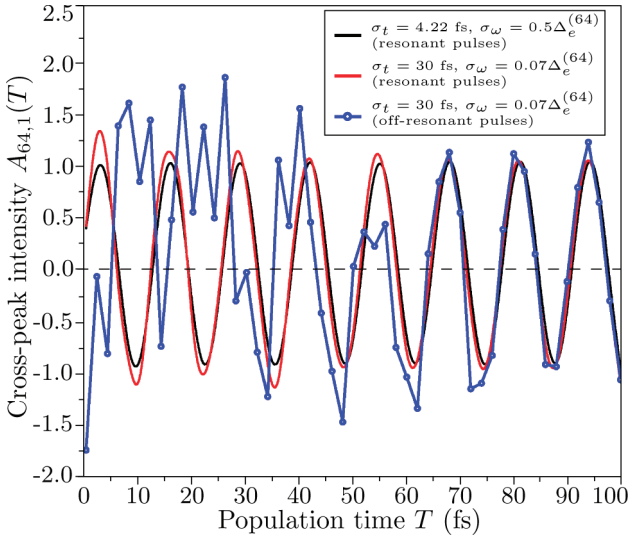

Figure 5. Cross-peak intensity $A_{64,1}$, as a function of delay time T defined from the 2C2D PE spectra, using resonant ($\{\omega_1, \omega_2, \omega_3\} = \{\varepsilon_{e_{64}}, \varepsilon_{e_1}, \varepsilon_{e_{64}}\}$) and off-resonant ($\{\omega_1, \omega_2, \omega_3\} = \{\varepsilon_{e_{64}} - 0.07\Delta_e^{(64)}, \varepsilon_{e_1} + 0.12\Delta_e^{(64)}, \varepsilon_{e_{64}} - 0.07\Delta_e^{(64)}\}$) broad- and narrow-bandwidth laser pulses, $\sigma_\omega = 0.5\Delta_e^{(64)}$ and $\sigma_\omega = 0.07\Delta_e^{(64)}$, respectively. The cross-peak intensity function is multiplied by a factor of 30 in the case of off-resonant pulses.

frequencies for the laser pulses, in comparison with the lowest and highest one-exciton energies of the single unit cell: $\{\omega_1, \omega_2, \omega_3\} = \{\varepsilon_{e_{64}} - 0.07\Delta_e^{(64)}, \varepsilon_{e_1} + 0.12\Delta_e^{(64)}, \varepsilon_{e_{64}} - 0.07\Delta_e^{(64)}\}$. Using such pulses, the amplitude of the $A_{64,1}(T)$ function dropped more than 30 times and the higher-frequency modulations appeared at times $T < 90$ fs for the laser pulses of the $\sigma_t = 30$ fs duration. This high-frequency contribution comes from the so-called double-coherence pathways. In the case of longer laser pulses, the pulse-ordered system−field interaction sequence might be broken. The system then can primarily interact with the third laser pulse $+\vec{k}_3$, followed by the interaction with the second pulse $+\vec{k}_2$, thus creating the coherence between the two-exciton state and the ground state $|f\rangle\langle g|$, which is later probed by the $-\vec{k}_1$ pulse. Despite the change in the wavevector order, the 2C 2D scheme is still $\{\omega_1, \omega_2, \omega_3\} = \{\varepsilon_{e_{64}}, \varepsilon_{e_1}, \varepsilon_{e_{64}}\}$. A double-coherence signal is expected for short delay times ($T < 3\sigma_t$).

CONCLUSIONS

The quantum coherence dynamics revealed in the two-dimensional (2D) spectra of the one-dimensional J-aggregates is studied. Such a model of the J-aggregate was proposed by Fidder,[36] from the detailed analysis of the absorption and fluorescence excitation spectra of concentrated water solution of the pseudo-isocyanine dye. Two-dimensional spectra of the unit cell of four molecules and the full-sized aggregate were theoretically analyzed using a system response function theory for the Frenkel-type excitons. Although this particular model was used in simulations, principles of spectral analysis and the conclusions would be essentially the same for the other aggregate systems.

Two-dimensional spectra of excitonically coupled dimer is well-known and all spectral elements can be unambiguously identified. In this paper, such identification of spectral elements for the four-molecule complex was presented: the cross-peaks can be addressed to quantum coherences of eigenstate motion

correlations, similar to that for a dimer system, while the induced absorption contributions produce negative spectral elements in the middle of the one-exciton band. From the position of the induced absorption elements, it is possible to justify the size of small molecular aggregates.

Two different methods of the inhomogeneous broadening simulation for the unit cell were assumed, either by using a direct inclusion of a slow bath motion mode in the spectral lineshape function (static homogeneous broadening) or by averaging over several realizations with random Gaussian-distributed chromophore energies (diagonal disorder). It is important to mention that the diagonal disorder partially enables the forbidden optical transition to the second eigenstate, which is not the case when using the static homogeneous broadening approach. However, the 2D spectra simulations provide similar results using both approaches. Thus, it can be concluded that both models provide identical spectra, except for the quantum coherence dynamics, where a slight increase of frequency of quantum beatings and long-lasting coherences are obtained when using the static homogeneous broadening approach, instead of diagonal disorder. Therefore, the model used for the system inhomogeneity simulations is very important for the quantum decoherence analysis, because it provides different coherence decay rates, while the static homogeneous broadening regime is sufficient to simulate other quantum phenomena as excitonic energy transfer pathways within the system.

The super-radiant J-band spectrum is a superposition of a few different pathways: induced absorption, population transfer, ground-state bleaching, and intraband quantum coherences. For the J-aggregate of PIC molecules, the J-band spectrum is essentially the same as that for the J-aggregates with a single molecule per unit cell, and no information regarding the structure of the single unit cell can be extracted.

The only evidence of a more-complex structure of the unit cell of the J-aggregate is the quantum coherences outside the J-band. Two-color two-dimensional spectroscopy can be successfully employed for probing quantum coherences of such systems with a broad excitonic band. In the case of resonant laser pulses, it was shown that the recorded cross-peak intensity function is not dependent on the pulse duration. For pulses being slightly off-resonant, the cross-peak intensity decreases significantly and the double-coherence contributions overwhelm the intensity dynamics. This property evidently resembles the J-aggregate structure.

AUTHOR INFORMATION

Corresponding Author

*E-mail: leonas.valkunas@ff.vu.lt.

ACKNOWLEDGMENT

This work was supported by the global grant of the Lithuanian Scientific Coucil according to operational programme of the Human Resources Development and the Lithuanian Scientific Council Student Research Fellowship Award (V.B., A.G.).

REFERENCES

(1) van Amerongen, H.; Valkunas, L.; van Grondelle, R. *Photosynthetic Excitons*; World Scientific: Singapore, 2000.
(2) Jelley, E. E. *Nature* **1936**, *138*, 1009.
(3) Scheibe, G. *Angew. Chem.* **1936**, *49*, 563.
(4) Fidder, H.; Knoester, J.; Wiersma, D. A. *J. Chem. Phys.* **1991**, *95*, 7880–7890.
(5) Kobayashi, T. *J-aggregates*; World Scientific: Singapore, 1996.
(6) Knapp, E. W. *Chem. Phys.* **1984**, *85*, 73–82.
(7) Malyshev, V. A.; Domínguez-Adame, F. *Chem. Phys. Lett.* **1999**, *313*, 255–260.
(8) Sundström, V.; Gillbro, T.; Gadonas, R. A.; Piskarskas, A. *J. Chem. Phys.* **1988**, *89*, 2754–2762.
(9) Fidder, H.; Knoester, J.; Wiersma, D. A. *Chem. Phys. Lett.* **1990**, *171*, 529–536.
(10) Fidder, H.; Knoester, J.; Wiersma, D. A. *J. Chem. Phys.* **1993**, *98*, 6564–6566.
(11) Johnson, A. E.; Kumazaki, S.; Yoshihara, K. *Chem. Phys. Lett.* **1993**, *211*, 511–515.
(12) Minoshima, K.; Taiji, M.; Misawa, K.; Kobayashi, T. *Chem. Phys. Lett.* **1994**, *218*, 67–72.
(13) Spano, F. C. *Chem. Phys. Lett.* **1994**, *220*, 365–370.
(14) Durrant, J. R.; Knoester, J.; Wiersma, D. A. *Chem. Phys. Lett.* **1994**, *222*, 450–456.
(15) Heijs, D.-J.; Dijkstra, A. G.; Knoester, J. Ultrafast Dynamics of Molecules in the Condensed Phase: Photon Echoes and Coupled Excitations—A Tribute to Douwe A. Wiersma. *Chem. Phys.* **2007**, *341*, 230–239.
(16) Spano, F. C.; Mukamel, S. *Phys. Rev. A* **1989**, *40*, 5783.
(17) Bakalis, L. D.; Knoester, J. *J. Phys. Chem. B* **1999**, *103*, 6620–6628.
(18) de Boer, S.; Vink, K. J.; Wiersma, D. A. *Chem. Phys. Lett.* **1987**, *137*, 99–106.
(19) de Boer, S.; Wiersma, D. A. *Chem. Phys. Lett.* **1990**, *165*, 45–53.
(20) Stiel, H.; Daehne, S.; Teuchner, K. *J. Lumin.* **1988**, *39*, 351–357.
(21) Cho, M.; Vaswani, H. M.; Brixner, T.; Stenger, J.; Fleming, G. R. *J. Phys. Chem. B* **2005**, *109*, 10542–10556.
(22) Zigmantas, D.; Read, E. L.; Mančal, T.; Brixner, T.; Gardiner, A. T.; Cogdell, R. J.; Fleming, G. R. *Proc. Natl. Acad. Sci. U.S.A.* **2006**, *103*, 12672–12677.
(23) Prall, B. S.; Parkinson, D. Y.; Fleming, G. R.; Yang, M.; Ishikawa, N. *J. Chem. Phys.* **2004**, *120*, 2537–2540.
(24) Cho, M.; Fleming, G. R. *J. Chem. Phys.* **2005**, *123*, 114506.
(25) Kjellberg, P.; Brüggemann, B.; Pullerits, T. *Phys. Rev. B* **2006**, *74*, 024303.
(26) Pisliakov, A. V.; Mančal, T.; Fleming, G. R. *J. Chem. Phys.* **2006**, *124*, 234505.
(27) Cheng, Y.-C.; Fleming, G. R. *J. Phys. Chem. A* **2008**, *112*, 4254–4260.
(28) Abramavicius, D.; Butkus, V.; Bujokas, J.; Valkunas, L. *Chem. Phys.* **2010**, *372*, 22–32.
(29) Brixner, T.; Stenger, J.; Vaswani, H. M.; Cho, M.; Blankenship, R. E.; Fleming, G. R. *Nature* **2005**, *434*, 625–628.
(30) Engel, G. S.; Calhoun, T. R.; Read, E. L.; Ahn, T. K.; Mančal, T.; Cheng, Y. C.; Blankenship, R. E.; Fleming, G. R. *Nature* **2007**, *446*, 782.
(31) Collini, E.; Scholes, G. D. *Science* **2009**, *323*, 369–373.
(32) Womick, J. M.; Miller, S. A.; Moran, A. M. *J. Phys. Chem. A* **2009**, *113*, 6587–6598.
(33) Milota, F.; Sperling, J.; Nemeth, A.; Kauffmann, H. Excited State Dynamics in Light Harvesting Materials. *Chem. Phys.* **2009**, *357*, 45–53.
(34) Stiopkin, I.; Brixner, T.; Yang, M.; Fleming, G. R. *J. Phys. Chem. B* **2006**, *110*, 20032–20037.
(35) Dijkstra, A. G.; la Cour Jansen, T.; Knoester, J. *J. Chem. Phys.* **2008**, *128*, 164511.
(36) Fidder, H. *Chem. Phys.* **2007**, *341*, 158–168.
(37) Abramavicius, D.; Palmieri, B.; Voronine, D. V.; Šanda, F.; Mukamel, S. *Chem. Rev.* **2009**, *109*, 2350–2408.
(38) Mukamel, S. *Principles of Nonlinear Optical Spectroscopy*; Oxford University Press: New York, 1995.
(39) May, V.; Kuhn, O. *Charge and Energy Transfer in Molecular Systems*; Wiley−VCH: Weinheim, Germany, 2004.
(40) Abramavicius, D.; Valkunas, L.; Mukamel, S. *Europhys. Lett.* **2007**, *80*, 17005.

(41) Abramavicius, D.; Palmieri, B.; Mukamel, S. *Chem. Phys.* **2008**, *357*, 79–84.
(42) Vaswani, H. M.; Stenger, J.; Fromme, P.; Fleming, G. R. *J. Phys. Chem. B* **2006**, *110*, 26303–26312.
(43) Yuen-Zhou, J.; Mohseni, M.; Aspuru-Guzik, A. http://arxiv.org/abs/1006.4866v2, accessed 2010.